PLOS ONE

RESEARCH ARTICLE

Collagen cross-links scale with passive stiffness in dystrophic mouse muscles, but are not altered with administration of a lysyl oxidase inhibitor

Sarah E. Brashear[1☯], Ross P. Wohlgemuth[1☯], Lin-Ya Hu[1], Elias H. Jbeily[2], Blaine A. Christiansen[2], Lucas R. Smith[1,3*]

1 Department of Neurobiology, Physiology, and Behavior, University of California Davis, Davis, California, United States of America, **2** Department of Orthopaedic Surgery, University of California Davis, Sacramento, California, United States of America, **3** Department of Physical Medicine and Rehabilitation, University of California Davis, Sacramento, California, United States of America

☯ These authors contributed equally to this work.
* lucsmith@ucdavis.edu

Citation: Brashear SE, Wohlgemuth RP, Hu L-Y, Jbeily EH, Christiansen BA, Smith LR (2022) Collagen cross-links scale with passive stiffness in dystrophic mouse muscles, but are not altered with administration of a lysyl oxidase inhibitor. PLoS ONE 17(10): e0271776. https://doi.org/10.1371/journal.pone.0271776

Editor: Andrew A. Voss, Wright State University, UNITED STATES

Received: July 6, 2022

Accepted: October 10, 2022

Published: October 27, 2022

Data Availability Statement: A spreadsheet with all the annotated data for this paper is available from figshare under the DOI (10.6084/m9.figshare.20234712).

Funding: This work was supported by National Institutes of Health (NIH) funded by the National Institute of Arthritis and Musculoskeletal and Skin Diseases (R00AR067867) to LRS. The funders had no role in study design, data collection and

Abstract

In Duchenne muscular dystrophy (DMD), a lack of functional dystrophin leads to myofiber instability and progressive muscle damage that results in fibrosis. While fibrosis is primarily characterized by an accumulation of extracellular matrix (ECM) components, there are changes in ECM architecture during fibrosis that relate more closely to functional muscle stiffness. One of these architectural changes in dystrophic muscle is collagen cross-linking, which has been shown to increase the passive muscle stiffness in models of fibrosis including the *mdx* mouse, a model of DMD. We tested whether the intraperitoneal injections of beta-aminopropionitrile (BAPN), an inhibitor of the cross-linking enzyme lysyl oxidase, would reduce collagen cross-linking and passive stiffness in young and adult *mdx* mice compared to saline-injected controls. We found no significant differences between BAPN treated and saline treated mice in collagen cross-linking and stiffness parameters. However, we observed that while collagen cross-linking and passive stiffness scaled positively in dystrophic muscles, collagen fiber alignment scaled with passive stiffness distinctly between muscles. We also observed that the dystrophic diaphragm showed the most dramatic fibrosis in terms of collagen content, cross-linking, and stiffness. Overall, we show that while BAPN was not effective at reducing collagen cross-linking, the positive association between collagen cross-linking and stiffness in dystrophic muscles still show cross-linking as a viable target for reducing passive muscle stiffness in DMD or other fibrotic muscle conditions.

Introduction

The mechanical function of skeletal muscle depends on the active contractile properties and the passive mechanics, both of which are compromised in muscle disease. Although there are several structures that contribute to the passive mechanics of skeletal muscle, one of the primary determinants is the extracellular matrix (ECM) [1–3]. The ECM contributes to passive

analysis, decision to publish, or preparation of the manuscript.

Competing interests: The authors have declared that no competing interests exist.

muscle stiffness largely through fibrillar collagen, specifically type I and type III [4]. Collagen has high tensile stiffness which produces passive tension in unstimulated muscle under strain and transmits the active forces produced by muscle contraction [5, 6]. The healthy ECM is critical to muscle function, however, in skeletal muscle diseases characterized by fibrosis such as Duchenne muscular dystrophy (DMD), there is a pathologic accumulation of ECM components which can cause excessive stiffness and often lead to joint contracture [7, 8]. Muscle contractures and loss of range of motion develop frequently in muscular dystrophies as a consequence of high muscle passive stiffness [9, 10]. Although contracture is a common symptom of fibrotic diseases, different muscles exhibit various degrees of dysfunction. The diaphragm is consistently the most severely affected by fibrosis, which contributes to respiratory failure and early mortality [11]. Although there are some surgical and physical remedies available to alleviate contractures of limb muscles, none of them reverse fibrosis and long-term efficacy is limited [12]. Therefore, there is a need to elucidate the molecular structures responsible for excessive muscle stiffness in order to develop targeted therapies for contracture in neuromuscular disorders.

While blocking collagen expression in rodent models of DMD has been accomplished [13], there are off-target effects and no anti-fibrotic therapy is approved for neuromuscular conditions. While the amount of collagen in muscle can contribute to its mechanical properties, other features of collagen architecture have been shown to be more critical in determining muscle stiffness. We have previously demonstrated that more nuanced qualities of the ECM, such as alignment, also hold strong predictive ability for both dynamic, velocity-dependent, and elastic, velocity-independent, passive muscle stiffness [14, 15]. Collagen cross-linking is feature of ECM organization that is known to contribute to stiffness and has been shown to increase in DMD and aged muscle [16, 17]. Collagen cross-linking inhibitors have been applied successfully in other fibrotic tissues [18–20], but have not been applied to skeletal muscle. Cross-links can be enzymatically formed through lysyl oxidase (LOX) and associated enzymes or through advanced glycation end-products (AGE) [18, 21, 22]. The frequency of collagen cross-linking varies between different muscles as does the plasticity of cross-link frequency in fibrosis [16]. Given their association with muscle passive stiffness and fibrosis, collagen cross-links are an attractive target for contracture therapy.

In this study we focused on inhibition of collagen cross-link formation as a therapeutic to reduce passive stiffness in skeletal muscle of *mdx* mice, a model for DMD. We used beta-aminopropionitrile (BAPN) as a naturally occurring inhibitor of the cross-linking enzyme LOX [23]. BAPN has been used in other mouse studies and shown to be well-tolerated and effective at reducing collagen cross-links in tissues other than muscle [20]. Importantly, LOX based collagen cross-linking is critical to bone integrity [24], but can be blocked with BAPN and is functionally impaired in dystrophic mice [25]. The *mdx* mice on the DBA/2J genetic background produce more severe fibrosis, thus more similar to the human condition than the *mdx* mice on the C57BL/6 background [26]. As fibrosis in the *mdx* DBA/2J strain is progressive [27], we utilized cohorts of young and adult mice to assess the preventative and reversal effects of BAPN treatment, respectively. While BAPN treatment was unsuccessful in inhibiting collagen cross-links in muscle, this study strengthens the muscle dependent association of ECM architecture with muscle stiffness.

Materials and methods

Ethical approval

All animal experiments were approved by the University of California, Davis Institutional Animal Care and Use Committee.

Table 1. Mouse sample size.

	Young		Adult	
	wildtype	*mdx*	wildtype	*mdx*
PBS	6 (3)	5 (2)	4 (2)	6 (3)
BAPN	6 (3)	6 (3)	5 (3)	7 (3)

N = total (female) mice.

https://doi.org/10.1371/journal.pone.0271776.t001

Animal handling and BAPN administration

DBA/2J (wildtype) and D2.B10-Dmd*mdx*/J (*mdx*) mice were housed and bred in the UC Davis Teaching and Research Animal Care Services (TRACS) facility. They were grouped and housed on a 12:12 light-dark cycle, and given ad libitum access to food and water. The mice were between 16–19 weeks (adult) and 4–5 weeks (young) of age when BAPN or PBS treatment was initiated with sample sizes listed in Table 1. 100 mg/kg/day of BAPN was administered through daily intraperitoneal injections for 4 weeks prior to sacrifice which has been shown to be an effective dose [20, 28]. Body mass was measured weekly.

Muscle isolation

Mice were anesthetized using 2.5% Isoflurane gas in 1 L/min of oxygen. After isolation of lower limb muscles, euthanasia by cervical dislocation was administered while mice were under anesthesia. Soleus, extensor digitorum longus (EDL), and diaphragm muscles were collected for isolated muscle contractile and passive mechanical measurements. Muscles were stored in Ringer's solution (Sodium Chloride, Potassium Chloride, Calcium Chloride dihydrate, Potassium Phosphate Monobasic, Magnesium Sulfate, 4-(2-Hydroxyethyl)piperazine-1-ethanesulfonic acid, Glucose) supplied with oxygen directly following collection and during mechanical testing. After passive and active mechanical testing, muscles from the left limb were flash frozen in liquid nitrogen and stored at -80˚C while muscles from the right limb were pinned at the estimated optimum muscle length (L_o) and fixed in 4% paraformaldehyde (PFA) for one day before storage in 4˚C PBS.

Passive muscle mechanics

The passive mechanical properties were measured as previously described [14]. Briefly, following isolation of EDL and soleus, 7–0 sutures were tied at the muscle-tendon junctions. A small strip of diaphragm was separated with knots tied at the central tendon and the ribs. The suture loops were secured to the 300C-LR-Dual-Mode motor arm and force transducer (Aurora Scientific) in a well of 20˚C Ringer's solution with bubbling oxygen [29, 30]. The L_o was ascertained through a series of twitches as the muscle was gradually stretched using the 701C stimulator (Aurora Scientific), with the length set at the maximum twitch amplitude [31]. The L_o length was measured using a caliper between the site where the sutures were tied (the proximal and distal muscle-tendon junctions). The muscle length (L_f), mass (m), ratio of fiber length to L_o (L_f/L_o), and density ($\rho = 1.06$ g/cm^3) were utilized to find the physiological cross-sectional area (PCSA) [32]: $PCSA = m/(L_o \cdot (L_f/L_o) \cdot \rho)$. PCSA was used to convert force values into stress for both stiffness measures and determination of specific tension in active muscle mechanics.

The strains that took place in the passive mechanical protocol were derived from the L_o. Before each strain the muscle was conditioned by periodic lengthening to the given strain at 1 Hz for 5 seconds (s). After conditioning, the muscle was stretched 2.5% at 1 L_o/s and kept at

the length for 120 s. Conditioning, strain, and relaxation was repeated at 5, 7.5, 10, and 12.5% strain. The elastic stiffness is the slope of the quadratic fit of elastic stress, the stress after 120 s of relaxation, at 10% strain [15]. Muscles that failed before the 10% strain were eliminated from the sample. Failure was determined as a drop in passive tension following an increase in strain, which indicates damage to passive elements within the muscle or the integrity of the attached suture. This technique is similar to other prior studies [15, 33–35].

Active muscle mechanics

Active mechanical protocols were performed on EDL and soleus muscles following passive mechanical measurement in Ringer's solution with bubbling oxygen. The active mechanical protocol consisted of measuring the maximum isometric twitch force (300 mA, 1.2 ms pulse width), allowing a 30 s rest, and measuring maximum isometric tetanus (300 mA, EDL: 0.3 ms pulse width, 120 Hz pulse frequency, 300 ms pulse train; SOL: 0.3 ms pulse width, 80Hz pulse frequency, 750 ms pulse train). This process was replicated two more times with 5 minutes between each bout of twitch and tetanus. The highest twitch and tetanus of the three trials was used in analysis.

Hydroxyproline assay

EDL, soleus, and diaphragm muscles from the left limb were measured for collagen content and cross-linking using the hydroxyproline and collagen solubility assay similar to other studies [15, 36, 37] and as described previously [14]. To begin the hydroxyproline assay, muscles were removed from -80˚C storage and powdered with mortar and pestle. Any remaining tendon tissue was removed from the muscle during powdering. The muscle powder was weighed, washed in 1 ml of PBS, and stirred for 30 minutes at 4˚C. After stirring, the powder and solution were centrifuged at 16,000g for 30 minutes at 4˚C. Following centrifugation, collagen that was not cross-linked was digested in a 1:10 (mass:volume) solution of 0.5M acetic acid containing 1 mg/ml pepsin, and was stirred overnight at 4˚C. The following day, the sample was centrifuged at 16,000 g for 30 minutes at 4˚C and the supernatant and pellet were separated. The supernatant contained the pepsin-soluble fraction (PSF) while the pellet contained the pepsin-insoluble fraction (PIF). Both the PSF and PIF were hydrolyzed in 0.5 ml of 6M HCl at 105˚C overnight. 10 μL of each sample was combined with 150 μL isopropanol and 75 μL of 1.4% chloramine-T (ThermoFisher) in acetate citrate buffer and oxidized for 10 min at room temperature. The samples were combined with 1 ml of 3:13 dilution of Erlich's reagent [1.5 g of 4-(dimethylamino) benzaldehyde (ThermoFisher); 5 ml ethanol; 337 μL sulfuric acid] to isopropanol and kept for 30 minutes at 58˚C. Each assay included a standard curve (0–1,000 μM trans-4-hydroxy-$_{L}$-proline; Fisher). Data were reported as μg hydroxyproline per mg powdered tissue wet mass.

Histological collagen architecture

Picrosirius red staining was done similarly to other studies [14, 15, 38, 39]. Before sectioning, fixed muscles were embedded in 4% agarose. 200 μm thick longitudinal sections were sliced using Leica VT1000S. Sections were washed, dried for 60 min, and stained for 60 min in 0.1% (weight/volume) Direct Red 80 (Fisher) dissolved in saturated aqueous picric acid (Fisher). Sections were washed twice for 60 s in 0.5% acetic acid, then dehydrated with three 60 s washes of 100% ethanol. The sections were then cleared using CitriSolv (Fisher Scientific) for 3 min, and blotted with Permount (Fisher Scientific).

Full longitudinal sections were imaged via a 20X objective with brightfield illumination on a Leica DMi8 microscope and DFC9000GTC camera. Linearly polarized light imaging

required a rotating polarizer in the beam path before and after the sample. A sequence of ten tiling scans were imaged at angles from 0 to 90˚ in increments of 10˚. ECM architecture was quantified using a custom MATLAB script providing MicroECM alignment and MacroECM deviation parameters as described previously [14] in conjunction with the polarized light images.

Second harmonic generation microscopy of collagen architecture

Second Harmonic Generation (SHG) microscopy samples were collected using similar 200 μm thick longitudinal sections as above. Sections were stained with RedDot 2 nuclear stain (Biotium) and WGA Oregon Green (Fisher). At the Advanced Imaging Facility in the UC Davis School of Veterinary Medicine, a Leica TCS SP8 fit with a Mai Tai deep see laser was used for SHG microscopy. A 25x water immersion objective was used for imaging in conjunction with the multiphoton laser, tuned to 870nm and 830nm in series. Sections were imaged three times at random locations to obtain images stacks with a total and slice thickness of 100 μm and 1 μm, respectively.

A custom MATLAB script and processing in ImageJ was used to analyze the images stacks as previously described [14, 40].

Trabecular and cortical bone microstructural properties

Following dissection, femurs were preserved in 70% ethanol and were imaged using micro-computed tomography (SCANCO Medical, μCT 35, Brüttisellen, Switzerland) to quantify trabecular bone microstructure at the distal metaphysis and cortical bone microstructure at the mid-diaphysis in accordance with the ASBMR guidelines for assessment of bone microstructure in rodents [41]. Bones were embedded in 1.5% agarose during imaging and were scanned with a 6 μm isotropic nominal voxel size (x-ray tube potential = 55 kVp, current = 114 μA, integration time = 900 ms). The μCT system was calibrated using standard density phantoms, and "bone" voxels were segmented from "non-bone" voxels using a global threshold of 471.3 mg HA/cm^3. Microstructural outcomes were directly measured by the manufacturer's analysis software, which uses the sphere distance transform method. Trabecular bone volumes of interest excluded the cortical shell and started adjacent to the metaphyseal growth plate extending 250 slices (1.5 mm) proximal. Trabecular bone volume fraction (BV/TV), trabecular thickness (Tb.Th), and other outcomes were determined for each bone. Cortical bone volumes of interest included 100 slices (600 μm) centered at the longitudinal midpoint of each femur. Cortical bone area (B.Ar), total cross-sectional area (Tt.Ar), and other outcomes were determined for each bone.

Bone 3-point mechanical testing

Following μCT scanning, femurs were mechanically tested in three-point bending to determine structural and material properties of cortical bone as recommended by the ASBMR guidelines for evaluating phenotypic changes in the diaphysis of long bones [42]. Bones were removed from 70% ethanol and rehydrated for 10–15 minutes in phosphate buffered saline (PBS) prior to mechanical testing using an electromagnetic materials testing system (ElectroForce 3200, TA Instruments, New Castle, DE) with the anterior aspect of each bone in tension. Data were collected at a sampling frequency of 50 Hz, the lower supports had a span of 5 mm, and the center loading plate was driven at 0.01 mm/sec until failure. Resulting force and displacement data were analyzed to determine structural properties of cortical bone (e.g., stiffness, yield force, ultimate force). Cross-sectional geometry at the mid-diaphysis determined from μCT was used to calculate material properties of cortical bone (e.g., elastic modulus, yield

stress, ultimate stress) using standard beam theory equations in accordance with established methods [42].

Statistical analysis

Images were analyzed while blind to their genotype and treatment. Z-score analyses were done within each muscle and then combined into groups based on treatment (PBS or BAPN) or age (young or adult). Three-way ANOVAs in GraphPad Prism were run by genotype (wildtype or *mdx*), age (young or adult), and treatment (BAPN or PBS) for each muscle. In cases where data were separated by sex, three-way ANOVAs by genotype, age, and treatment were performed separately within male and female groups. Post-hoc Sidak multiple comparison tests were done in GraphPad Prism to discover differences between individual groups. Correlations and linear regressions were performed in GraphPad Prism on pairs of quantitative data. Stepwise multiple linear regressions models were generated in MATLAB with significance to enter the model set to $p<0.10$ and significance to exit the model set to $p<0.20$. Unless otherwise stated, significance was set at $p<0.05$. In the figures, significance bars represent significant main effects determined by three-way ANOVAs for treatment, genotype, and age. Significance symbol above groups indicates significance from corresponding genotype according to post-hoc Sidak multiple comparisons tests.

Results

Muscle mass and function

Prior to muscle isolation, the body weight of the mice was recorded. All skeletal muscles of the *mdx* mice were impacted, but the diaphragm was grossly altered with highly fibrotic regions interspersed within muscle (Fig 1A). As expected, there was an increase in body mass in the adult mice compared to the young (Fig 1B). BAPN led to decreased body weight in *mdx* mice. We compared the limb muscle mass relative to the overall body weight and noted increases in both *mdx* soleus muscles compared to the wildtype soleus (Fig 1C). However, the EDL did not exhibit changes in muscle mass relative to body weight by age, treatment, or genotype (S1A Fig). As expected, the specific tension generated by the limb muscles during maximum isometric tetanus was significantly reduced in both the soleus (Fig 1D) and EDL (S1B Fig) but was not affected by BAPN treatment in any muscle or age. The passive elastic muscle stiffness of the *mdx* diaphragm was significantly increased compared to wildtype as anticipated (Fig 1E), but again BAPN had no impact on muscle stiffness. Neither did BAPN impact limb muscle elastic stiffness, although in soleus muscle there was a significant increase in elastic stiffness with age across conditions. The resistance to the initial stretch, dynamic stiffness, was similar to changes in elastic stiffness, but with an even more pronounced increase in the *mdx* diaphragm (S1B Fig). The elastic index or ratio of elastic to dynamic stiffness thus decreased as *mdx* diaphragm became less elastic in *mdx* mice (Fig 1F). The elastic index also decreased with age in *mdx* diaphragms. In the soleus however, the *mdx* muscles became significantly more elastic further indicating the muscle specific impacts. So, while the functional impact of *mdx* was muscle specific with decreased specific tension and increased stiffness in a muscle dependent manner as anticipated, treatment with BAPN did not induce significant changes to muscle function.

Collagen content and cross-linking

As expected, there was a dramatic increase in collagen of the adult *mdx* diaphragm compared to wildtype with a significant, but moderate increase in collagen in the EDL (Fig 2A). The

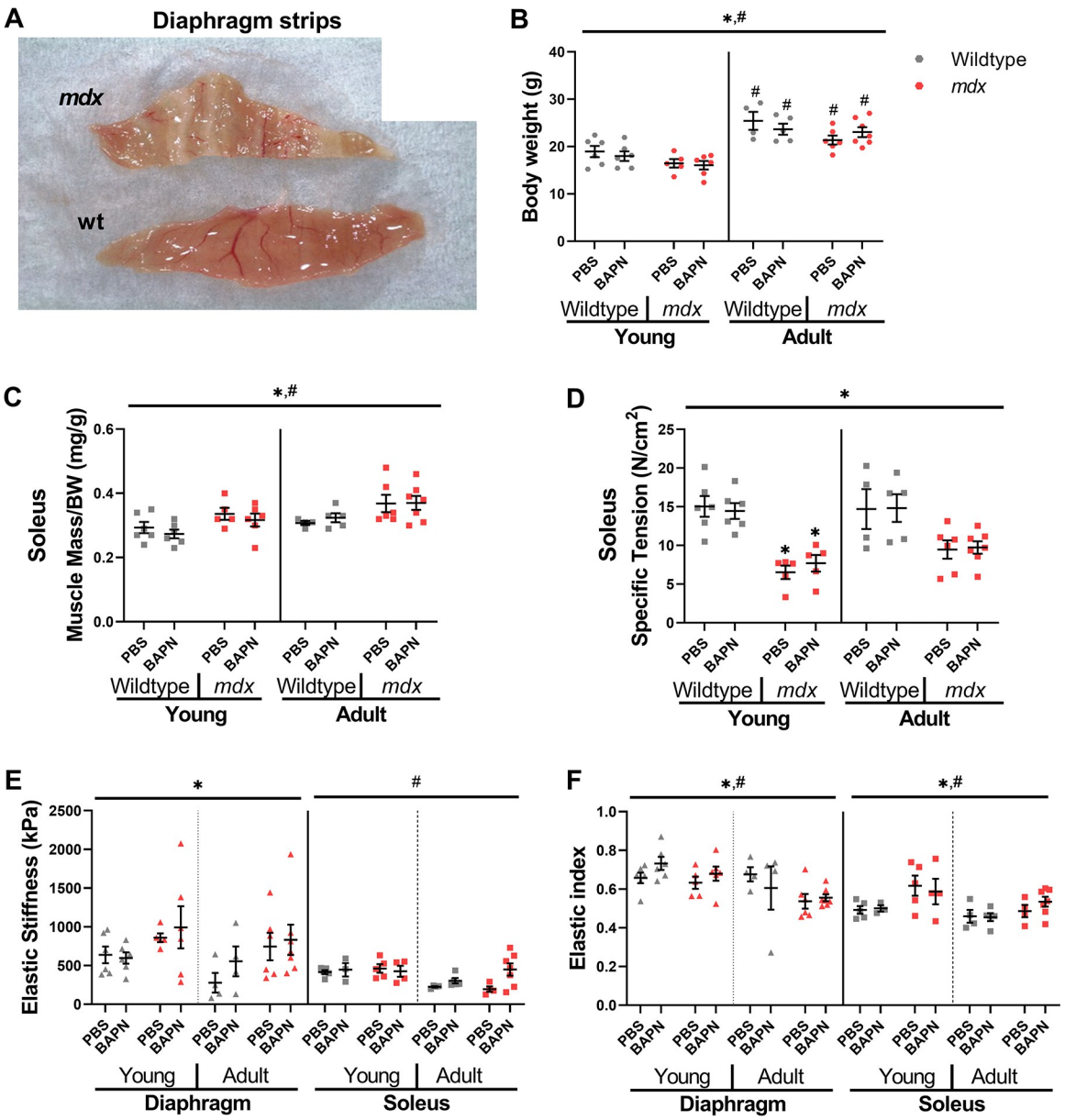

Fig 1. BAPN and muscle mechanics in wildtype and *mdx*. (A) Representative image of isolated wildtype and *mdx* diaphragm (DP) muscles for ex vivo mechanical testing. (B) Total body weight was greater for adult mice than young mice in both *mdx* and wildtype. (C) In soleus, there were significant effects of age and genotype on muscle mass. (D) The specific tension of *mdx* soleus muscles were significantly lower than wildtype. (E) Elastic stiffness taken as the elastic modulus at 10% strain showed *mdx* diaphragm was significantly stiffer than the wildtypes, and young soleus was significantly stiffer than adult soleus. (F) Elastic index, related to the amount of force remaining after stress relaxation compared with the peak force, showed significant effect of age and genotype in diaphragm and soleus muscles. * = genotype effect, # = age effects, * = $p<0.05$ determined by three-way ANOVAs with post-hoc Sidak multiple comparisons tests.

https://doi.org/10.1371/journal.pone.0271776.g001

wildtype diaphragm collagen didn't increase into adulthood, but in the case of *mdx* there was a substantial increase as diaphragm fibrosis onset. In the EDL muscle, collagen increased with age for both genotypes. Insoluble collagen represents more maturely cross-linked collagen and followed a similar pattern of being increased in *mdx* and adult muscles and was significant in diaphragm and EDL muscles (Fig 2B). The insoluble collagen percentage is an index of the

relative extent of collagen cross-linking. Collagen cross-linking was increased in the *mdx* mice diaphragms for both age groups and muscles. However, despite BAPN's function to inhibit cross-linking, treatment did not impact relative collagen cross-linking for any group (Fig 2C). Despite the ineffectiveness of BAPN in inhibiting collagen cross-linking in the muscle the natural variation in collagen and cross-linking could impact the measured elastic stiffness. Across muscles and within the *mdx* muscle in particular, there was a positive relationship between stiffness and total collagen (Fig 2D), cross-linked insoluble collagen (Fig 2E), and relative cross-linking as percent insoluble (Fig 2F). However, we did not observe a significant relationship between collagen content or cross-links and passive stiffness across wildtype muscles. Although the correlations across muscles and within *mdx* were modest, they were highly significant. Importantly, cross-linked collagen was more tightly associated than total collagen while relative extent of cross-linking was most well associated with stiffness. These associations support that collagen cross-linking contributes to muscle stiffness, but BAPN treatment was not effective in reducing collagen cross-linking.

Collagen alignment with polarized light microscopy

Thick (200 μm) longitudinal vibratome cut sections were stained with Sirius red and imaged them with polarized light microscopy to look at alignment on a subpixel scale (MicroECM alignment) and across the section (MacroECM deviation) (Fig 3A). There were no significant differences related to age, genotype, or BAPN treatment when looking at MacroECM deviation, the inverse of ECM alignment (Fig 3B, S2B Fig). Interestingly, there was a highly significant drop in MicroECM alignment in the adult diaphragms of both wildtype and *mdx* mice, but this was not observed in limb muscles (Fig 3C, S2A Fig). MacroECM deviation did not correlate with elastic stiffness overall (Fig 3D) and neither did MicroECM alignment (Fig 3E). This was in contrast to a previous study from our lab where we observed a negative correlation between macroECM deviation and elastic stiffness in the wildtype muscles [14]. Interestingly, MicroECM alignment did correlate with elastic index negatively in the soleus ($R^2 = 0.3140$) (S2C Fig). There was also a weak correlation between elastic index and MacroECM deviation across all muscles ($R^2 = 0.055$) (S3D Fig). Thus, polarized light microscopy did not identify any impacts of BAPN treatment, but demonstrated an age-related shift in diaphragm ECM microarchitecture.

Collagen architecture with second harmonic generation microscopy

Representative images show different patterns of collagen orientation within the muscle with variable alignment, fiber size, and fiber area (Fig 4A, S3A Fig). Collagen deviation, the inverse of collagen alignment, was decreased in *mdx* EDL as previously observed [14] and adult soleus (Fig 4B, S3C Fig). However, the fibrotic diaphragm showed no differences in collagen deviation between age, genotype, or treatment. Collagen fiber area was significantly increased in the adult *mdx* diaphragm compared to the wildtype corresponding to the high collagen and severe fibrosis (Fig 4C). While limb muscles collagen fiber area was not significantly changed by dystrophy, there were significant increases in collagen fiber area with age in the EDL and soleus (Fig 4C, S3B Fig). Collagen fiber size was not significantly different among groups in the diaphragm, but there was a significant effect of age such that there were larger collagen fibers in the adult soleus compared to the young (S3E Fig). The collagen alignment could be a function of tissue strain, which can be captured by sarcomere length measurements obtained by SHG microscopy. There was a weak but significant positive correlation between sarcomere length and collagen deviation across all muscles and in the diaphragm (All: $R^2 = 0.0369$, DP: $R^2 = 0.1210$) (S3F Fig), but with no changes in sarcomere length between groups the resting

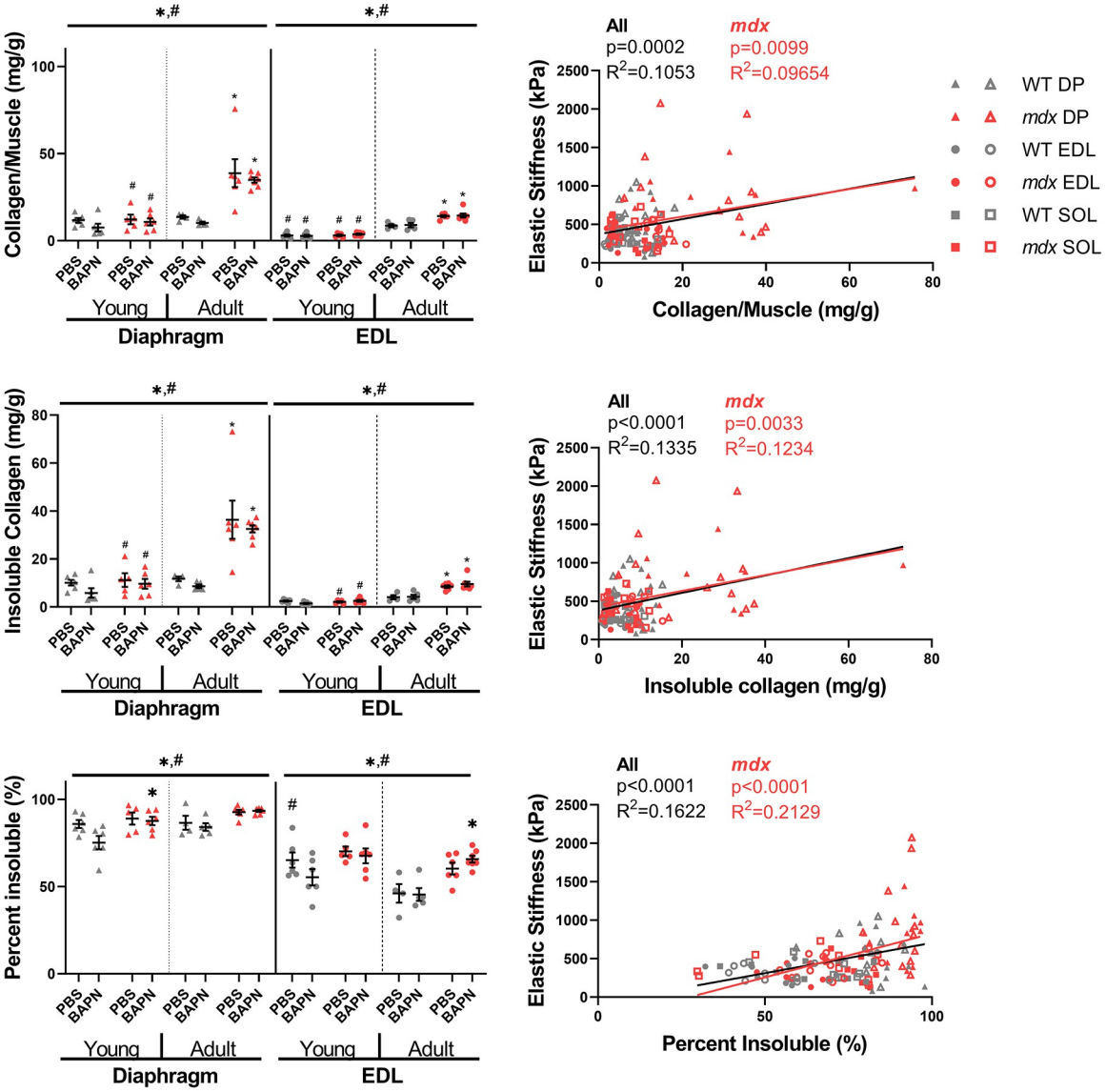

Fig 2. Collagen content and cross-linking. BAPN did not reduce collagen cross-links and the *mdx* diaphragm showed the most extensive fibrosis in terms of collagen content and cross-links. (A) The amount of collagen per muscle in wildtype and *mdx* muscles. The diaphragms and EDL muscle collagen content of *mdx* mice was significantly increased compared with the wildtype. (B) Insoluble (cross-linked) collagen was higher in *mdx* and adult muscles compared to wildtype. (C) The percentage of collagen that was cross-linked was higher in the *mdx* diaphragm and EDL muscles compared to the wildtype. Percent insoluble collagen was higher in the adult diaphragm and lower in the adult EDL compared to the respective young muscles. (D-F) Total collagen, insoluble collagen, and percent insoluble collagen scaled with elastic stiffness across all muscles together and the set of *mdx* points. * = genotype effect, # = age effects, * = $p<0.05$ determined by three-way ANOVAs with post-hoc Sidak multiple comparisons tests.

https://doi.org/10.1371/journal.pone.0271776.g002

sarcomere length is unlikely to drive effects in this study (S3D Fig). Collagen architecture measured by SHG was also significantly correlated with elastic stiffness, although the trends varied by muscle. Across muscles collagen deviation scaled positively with elastic stiffness (R^2 = 0.0673), which was the opposite of the hypothesized relationship. Notably, in the EDL lower collagen deviation and thus more aligned collagen was correlated with higher stiffness as predicted (R^2 = 0.1227) but, there were no significant correlations between collagen deviation and elastic stiffness in the diaphragm and soleus (Fig 4D). On the other hand, collagen fiber area scaled positively with elastic stiffness overall (R^2 = 0.0701) as would be expected, but the effect

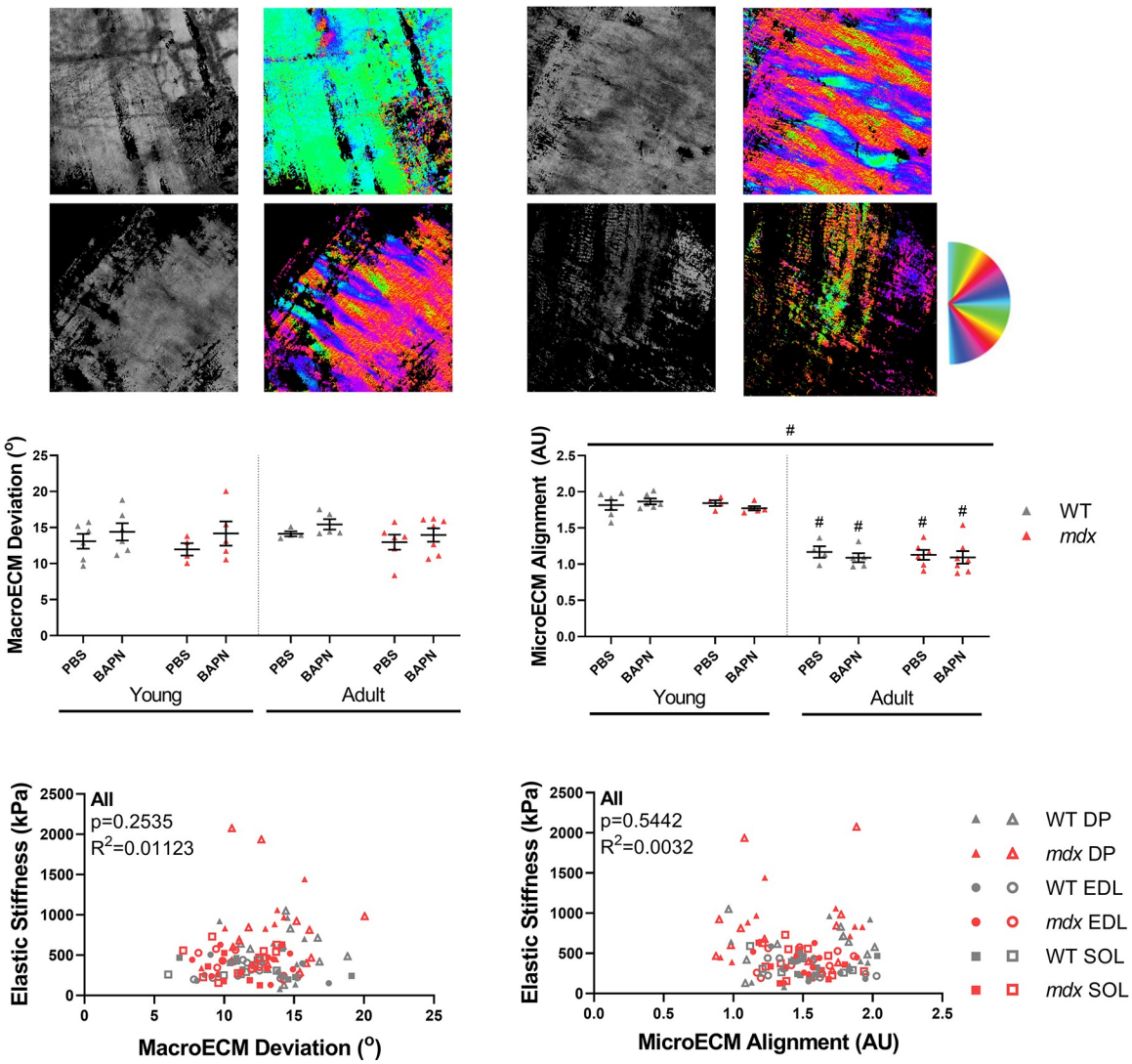

Fig 3. Sirius red collagen architecture. The *mdx* diaphragm had a decrease in microECM alignment compared to wildtype, but this was not correlated to a change in elastic stiffness. (A) Representative images of MicroECM alignment (left) and MacroECM deviation (right) in wildtype and *mdx* diaphragm muscles. (B) The MacroECM deviation showed no significant differences between genotypes or ages in the diaphragm. (C) The quantification of the MicroECM alignment showed significant differences between young and adult in both wildtype and *mdx* diaphragms. (D) The relationship between MacroECM alignment and elastic stiffness showed no significant correlation overall or in individual muscles. (E) There was no significant relationship between MicroECM deviation and elastic stiffness overall or in any individual muscle. Significance bar represents significant main effect as determined by three-way ANOVA across treatment, genotype, and age. Significance symbol above groups indicates significance from corresponding genotype or age group according to post-hoc Sidak multiple comparisons tests. # = age effects, # = $p<0.05$.

https://doi.org/10.1371/journal.pone.0271776.g003

was not present within individual muscles (Fig 4E). Direct visualization of collagen fibers again failed to show an impact of BAPN. Importantly however, this method did show unique adaptations by muscle where increased collagen alignment contributed to *mdx* EDL stiffness where more collagen fibers drive stiffness in adult *mdx* diaphragm.

Relationships between collagen architecture and muscle function

To form a holistic view of how each ECM parameter related to functional parameters as well as other ECM parameters correlation matrices were made for all muscles and within each muscle

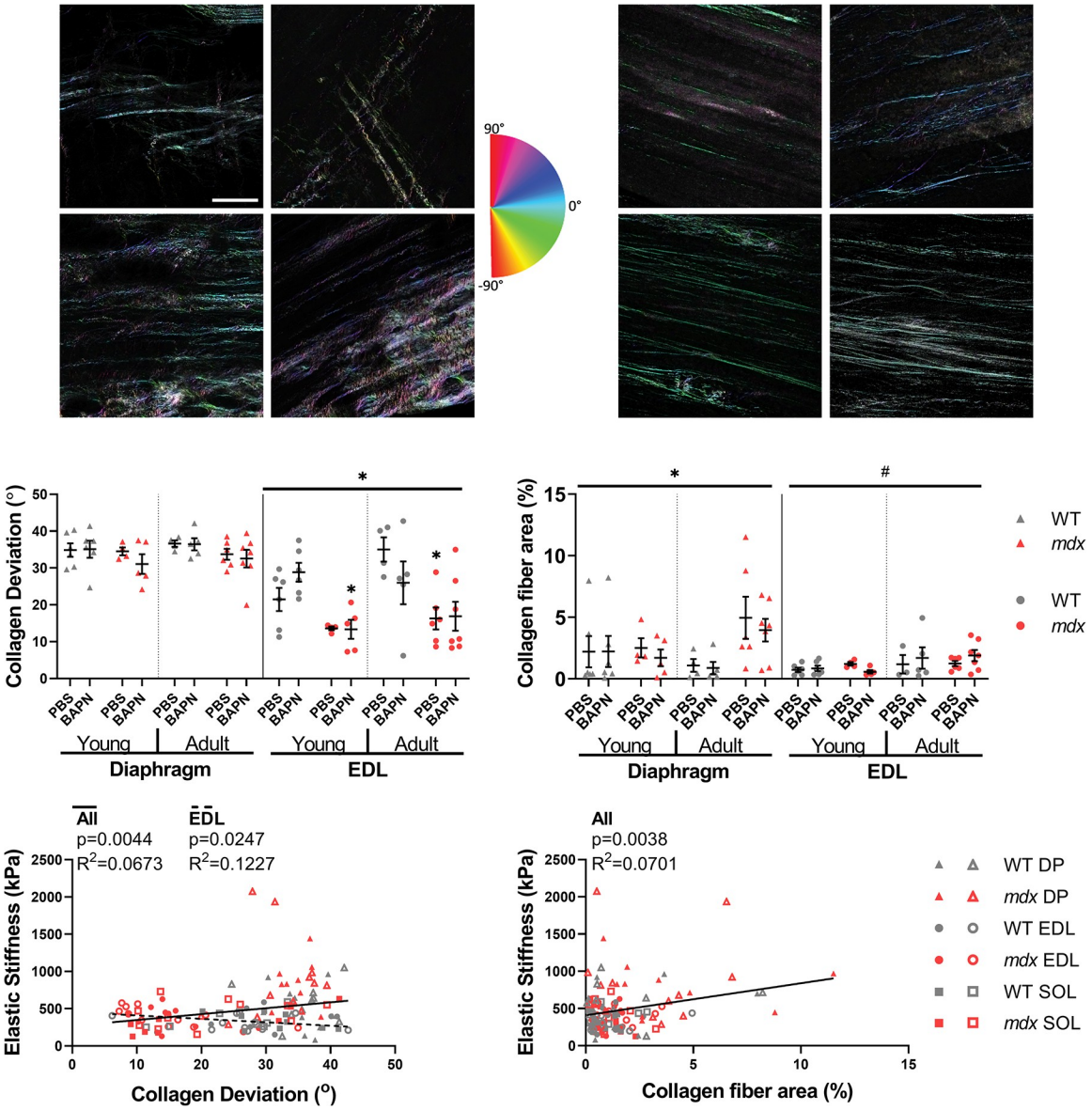

Fig 4. Second harmonic generation collagen architecture. Collagen architecture is altered in dystrophic muscle and relates to passive mechanics. (A) Second Harmonic Generation (SHG) representative images of diaphragm and EDL muscle sections from young, adult, wildtype, and *mdx* mice. Colormap represents angles of each pixel window in the images as analyzed by OrientationJ. Scale bar is 100μm. (B) The *mdx* EDL had significantly lower collagen deviation (higher alignment) compared to the wildtype. (C) Collagen fiber area was increased in *mdx* diaphragms compared to wildtype. Adult EDL muscles had higher collagen fiber area than young EDL muscles. (D) All groups combined had a significant positive correlation of collagen deviation and elastic stiffness. The EDL had an independent significant negative correlation. (E) Collagen fiber area correlated positively with elastic stiffness across all muscles. Significance by genotype: $^{*}p<0.05$and age: #$p<0.05$.

https://doi.org/10.1371/journal.pone.0271776.g004

group (S4A–S4D Fig). While many significant relationships were observed, in order to determine which were most prominent and non-redundant multiple linear regressions were run across and within muscles. Over all muscles the most powerful predictor was the percentage of cross-linking while the amount of cross-linked collagen contributed independently as well (Fig 5A). The collagen deviation entered into the model also, but surprisingly with more deviation, or less alignment, leading to more stiffness. These relationships can be driven by independent

differences between muscles. Within the EDL in particular, the relationship to collagen deviation was as expected and previously observed with more alignment leading to more stiffness (Fig 5B). The largest predictor in the EDL however, the area of collagen in perimysium fibers. In the EDL having less soluble non-cross-linked collagen was a predictor for stiffness likely related to less collagen cross-linking. In soleus muscles the relationship of elastic stiffness to collagen deviation was again reversed, albeit somewhat weaker (Fig 5C). Notably, the diaphragm did not produce a significant model overall although in the adult diaphragm sarcomere length, collagen fiber area, and fiber size were all positive predictors of stiffness (S5E Fig). Linear models were also run for adult and young muscles against elastic stiffness which showed fiber size, fiber area, and insoluble collagen as common positive predictors for stiffness (S5D–S5I Fig). These models were comparable to those of dynamic stiffness which gave insoluble collagen and soluble collagen as common positive and negative predictors of stiffness, respectively (S5J–S5M Fig). When linear models were made to predict specific tension in the EDL and soleus, the combined model gave insoluble collagen as a negative predictor of strength (S5A Fig). The EDL model had collagen deviation as a contributor to specific tension in addition to less insoluble collagen (S5B Fig) while the model for the soleus gave sarcomere length as a positive predictor for specific tension (S5C Fig). Together, these relationships indicate that collagen architecture is more predictive of muscle stiffness than total collagen content, collagen cross-linking is a consistent contributor to stiffness, and collagen alignment has a muscle specific influence on stiffness.

Dystrophic bone morphology and mechanics

Mid-diaphyseal total cross-sectional area of the femur determined by μCT (Fig 6A) showed substantial increase with age as expected, along with an increase in *mdx* mice compared to wildtype mice for both males and females (Fig 6B). However, BAPN did not have a large impact on bone cross-sectional area except potentially in the young *mdx* males. The cortical bone area had a similar effect of age, but was lower in *mdx* mice, particularly in adults (Fig 6C and 6D). Again, BAPN impact was isolated and in this instance to the young female *mdx* mice. Trabecular thickness also dramatically increased with age and was decreased broadly in *mdx* femurs (Fig 6E). Importantly, BAPN significantly lowered trabecular thickness in female mice. Conversely, trabecular bone volume fraction did not change with age or BAPN treatment but was depressed in *mdx* mice (Fig 6F).

Unsurprisingly, bones from adult mice exhibited substantially higher elastic modulus (Fig 6G) and ultimate stress than in young mice (Fig 6H). Female *mdx* mice had significantly lower stiffness and ultimate stresses, but in males the *mdx* effect was less consistent. Importantly, the modest impact of BAPN on bone structure did not contribute to any defect in bone mechanical properties. These bone analyses substantiate age related defects in *mdx* mice that are more prominent in females but with only a minor impact of BAPN on bone morphology with the applied treatment conditions.

Discussion

Although BAPN administration did not generate meaningful differences in skeletal muscle properties compared to PBS, there were notable shifts in the ECM architecture with dystrophy by muscle and age that have not previously been described. While expected differences were present with age such as greater body weight and muscle mass, there were notable distinctions such as lower elastic stiffness and elastic index in the adult muscles versus young. Two of the most robust age, genotype, and muscle-specific differences were the levels of collagen content and cross-linking. All muscles showed significant effects of age related to percent insoluble,

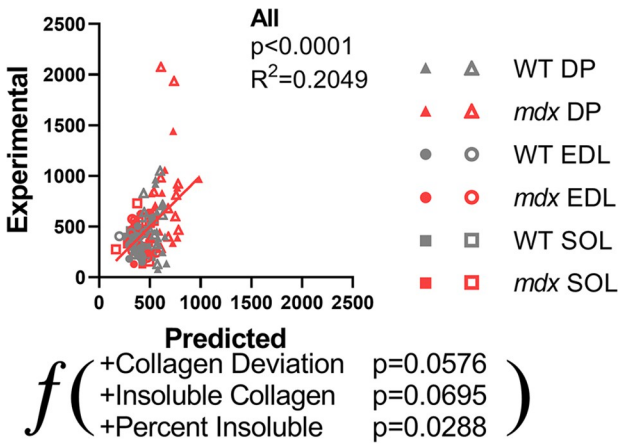

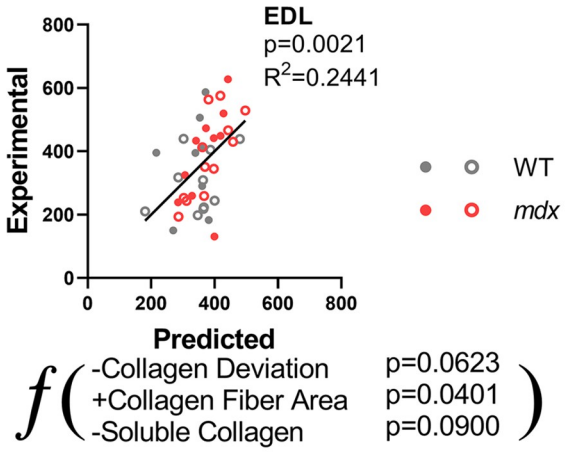

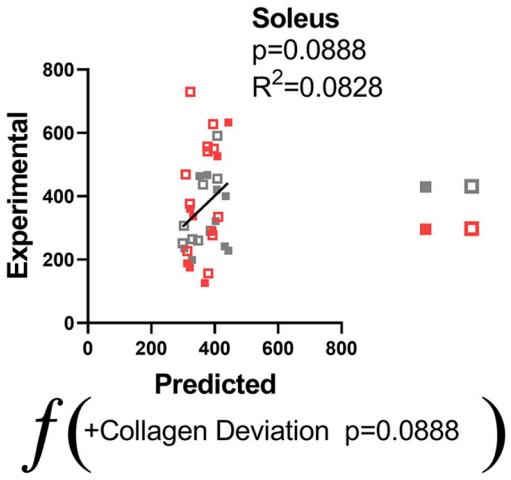

Fig 5. Multiple linear regressions for elastic stiffness. Aspects of collagen architecture predict elastic stiffness across muscles and within EDL and soleus. (A) A multiple linear regression model was run in MATLAB to predict elastic stiffness across all muscles and individually within each muscle. The model produced significant predictors collagen deviation, insoluble collagen, and percent insoluble. (B) Collagen deviation and soluble collagen were negative predictors and collagen fiber area was a positive predictor of EDL elastic stiffness. (C) Collagen deviation was a positive predictor of elastic stiffness in the soleus.

https://doi.org/10.1371/journal.pone.0271776.g005

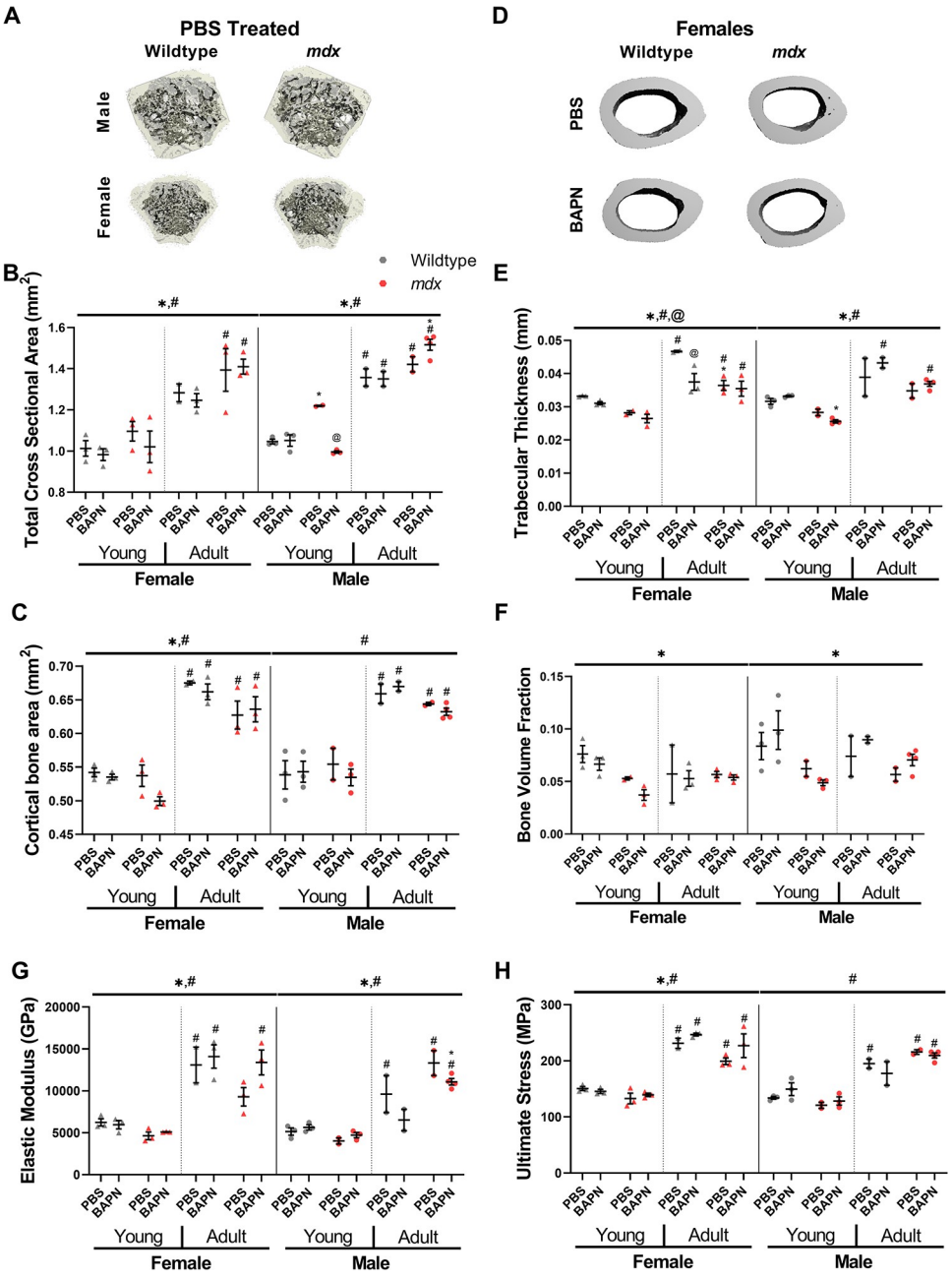

Fig 6. Microstructual and mechanical properties of long bones. (A) Representative images of mid-diaphyseal total cross-sectional area of the femur by μCT. (B) Total cross-sectional area was significantly increased in adult and *mdx* mice. (C) Cortical bone area was significantly increased in both male and female mice, and female mice also showed decreased area in *mdx* mice. (D) Representative images of cortical bone area. (E) There was an increase in trabecular thickness in adult mice, and a decrease in *mdx* mice. BAPN also decreased thickness in adult female wildtype mice. (F) Trabecular bone volume fraction was decreased in *mdx* mice. (G) Adult mice had significantly increased elastic modulus. (H) Adult mice had significantly increased ultimate stress. Significance by genotype: $^{*}p<0.05$, age: #$p<0.05$, and treatment: @$p<0.05$ determined by three-way ANOVA test with post-hoc Sidak multiple comparisons tests.

https://doi.org/10.1371/journal.pone.0271776.g006

insoluble collagen content, and total collagen while the EDL and diaphragm showed increases in those parameters in the *mdx* mice compared to wildtype. In all muscles the adult groups trended higher than the young for more cross-linked and total collagen content. This led to a

higher proportion of collagen cross-linking in the adult diaphragm, but surprisingly, in the fast-twitch EDL the effect of age was reversed, with lower cross-linking in adult mice. Compared to limb muscles, the diaphragm showed the greatest amount of collagen content and cross-linking. This was greatly amplified in *mdx* diaphragm in line with previous studies showing severe fibrosis [14, 16, 43] and critical with diaphragm function dramatically compromised in DMD leading to progressive respiratory insufficiency [44, 45]. Further, the high collagen content in the diaphragm, specifically in the *mdx* mice, likely drove the positive correlation between total collagen and elastic stiffness which was shown to be negative for the EDL and soleus in a previous study from our lab [14]. Diaphragm muscles also show dramatic impairment in active mechanical properties not measured here [27, 46], but which are also compromised by fibrosis. This more robust characterization of the altered ECM architecture in the diaphragm emphasizes the need to discover anti-fibrotic therapies that effectively target the diaphragm in DMD to preserve diaphragm function throughout the lifespan.

The use of SHG microscopy was well suited to directly visualize the sarcomeric and collagen structure of the muscle. This study is the first to investigate the alignment of perimysial collagen fibers in the diaphragm. However, this aspect of architecture was not significantly altered in dystrophic mice as opposed to previous observation of limb muscles [14]. Furthering the distinctions, across muscles increased alignment led to less stiffness. This was contrary to the previous investigation, but was driven by inclusion of the relatively high stiffness and high deviation of collagen in the diaphragm. The consistency of collagen alignment as a driving factor in the EDL stiffness further distinguished the uniqueness of the diaphragm. This points to the distinct relationship between collagen architecture and stiffness in different muscles. As with biochemical measures of collagen, the amount of perimysial collagen fibers measured by SHG were increased most prominently in the *mdx* diaphragm, but not until adulthood and not in the limb muscles. There is evidence that the collagen cables in the perimysium are important to the overall muscle mechanical properties and undergo changes in fibrosis that confer increases in tissue stiffness [3, 14, 47, 48]. While the amount of collagen in skeletal muscle is not always a consistent predictor of tissue stiffness [14, 15, 49], collagen fiber area seems to be relevant to the mechanical properties in some muscles given its incorporation in the multiple linear regressions of the overall EDL, adult EDL, and adult diaphragm and as demonstrated previously [14]. Collagen fiber size was a positive predictor for elastic stiffness in multiple linear models including the adult overall, adult diaphragm, and young EDL groups. While perimysial collagen fibers are only a subset of overall collagen, the importance of collagen fiber area and the alignment of those collagen fibers in determining stiffness highlight their important role in passive muscle function and as targets for anti-fibrotic therapies.

A wrinkle to the mechanism of dystrophic damage of the diaphragm includes its fan shape that incurs strains in multiple directions. One possibility is that given its low level of collagen alignment compared to the limb muscles, the diaphragm's stiffness may be more dependent on its level of collagen content and cross-linking. In the multiple linear regression for elastic stiffness, the adult diaphragm included sarcomere length, collagen fiber area, and collagen fiber size as positive predictors while the regression for dynamic stiffness generated insoluble collagen as the only positive predictor for the overall and adult diaphragm. These models show ECM parameters of collagen cross-linking, fiber area, and fiber size as useful predictors for diaphragm stiffness, although the relevance of these parameters across aging is still unclear. Paired with the observation that the diaphragm collagen fibers are less aligned than those of the EDL and soleus, it may be the case that this alignment or lack thereof may play a role in the diaphragm's stiffness in a different axis. This could also help explain why diaphragm alignment does not significantly relate to stiffness since we mechanically tested the diaphragm muscle along the myofiber angle. While some experiments have been done to estimate or directly

measure diaphragm mechanics in the transverse axis [50, 51], further experiments testing diaphragm mechanical properties in multiple directions of strain and relating them to collagen architecture would further elucidate this relationship.

This study was designed to block collagen cross-linking in skeletal muscle. BAPN has been previously shown to be an effective collagen cross-linking inhibitor in multiple tissues [23, 52] and similar effects in muscle were anticipated. The dosage of 100 mg/kg/day and intraperitoneal delivery method were similar to previous experiments showing effectiveness of BAPN in blocking collagen cross-linking [28, 53]. The moderate impact on bone morphology and trabecular thickness in particular supports that the BAPN dosage was active to some extent. However, studies looking at the impact of BAPN in bone have used higher concentrations, such as 200 mg/kg/day or 500 mg/kg/day [24]. Thus, increasing the dose may be necessary to elicit collagen cross-linking inhibition in musculoskeletal tissues [54, 55]. Injecting the BAPN locally into the muscle may more effectively inhibit collagen cross-linking by allowing for high local concentrations, but repeated injections could be a significant source of injury. Alternative collagen cross-linking inhibitors may be more effective in skeletal muscle. The usage of neutralizing antibodies to the collagen cross-linking enzyme, lysyl oxidase like 2, have been shown to block collagen cross-linking in lung, liver, and kidney fibrosis [56–60]. While BAPN was ineffective at blocking collagen cross-linking in this study, the results still advocate for effective inhibition of collagen cross-linking as an efficacious way to reduce muscle stiffness and contractures.

There are several aspects of our study that limit the interpretations of the data. One such limitation is the absence of a lysyl oxidase activity assay to measure the effectiveness of BAPN to inhibit lysyl oxidase. Although we did not utilize a lysyl oxidase activity assay in this study, future investigations could use newly developed assays to assess if BAPN is effective in inhibiting cross-linking enzymes in skeletal muscle compared to other tissues [61]. While lysyl oxidase activity assays are commercially available the applicability to in vivo activity is questionable due to the processing steps required [61]. Thus, our end-point measurements of collagen cross-linking provide the most direct evidence that lysyl oxidase was not inhibited by BAPN in the muscle ECM. As with all mouse models of DMD the severity and degree of fibrosis is less than the human condition. However, we utilized a more severely fibrotic mouse model with the *mdx* mutation on the DB2 background to produce a more fibrotic phenotype [26, 27]. Another limitation is the linear strain placed on the diaphragm compared to how the diaphragm functions *in vivo*. Bi-axial investigation of the diaphragm passive mechanics may yield new insights into the unique collagen architecture. While measuring collagen architecture and mechanics in the same muscles provides greater power, the imaging is only performed on a small section of the muscle. For polarized light imaging few differences were observed, and the change in micro-alignment with age specifically in the diaphragm is difficult to interpret. For SHG-based measures, only the perimysium collagen fibers were analyzed, while contributions from the epimysium and endomysium were not incorporated. Despite these limitations this study provides the most comprehensive investigation of skeletal muscle passive mechanics dependence on ECM architectural features to date.

Despite the inability to evaluate the influence of reduced collagen cross-linking on muscle mechanics as intended, this study provides a robust analysis of ECM features and muscle stiffness across dystrophy, age, and muscles. This led to discovery that while the EDL muscle stiffness is closely related to collagen alignment is a major factor in muscle stiffness, dystrophic diaphragm muscle stiffness is more dependent on increased collagen content and cross-linking. This emphasizes that while the ECM response to muscular dystrophy is relatively consistent across muscles, with more collagen, cross-linking, and alignment, the implications for stiffness are muscle dependent. This study furthers our knowledge of the determinants of

passive muscle stiffness and is critical for future efforts evaluating anti-fibrotic therapies in models of muscular dystrophy for their impact on muscle function and stiffness.

Supporting information

S1 Fig. EDL muscle mechanics and dynamic stiffness. *Mdx* EDL showed a reduction in specific tension with no change in elastic stiffness. (A) There was no significant effect of genotype, age, or treatment on muscle weight in the EDL. While the standard *mdx* model often shows a pseudohypertrophy of limb muscle, the D2.*mdx* mouse muscle does not experience the increase in muscle mass [27]. (B) Specific tension during a maximal tetanus was reduced in the *mdx* EDL compared to wildtype. (C) Dynamic stiffness was increased in *mdx* in the diaphragms and was also increased in the young soleus compared to adult. There was no main effect of treatment, age, or genotype on the EDL dynamic stiffness. (D) There was no main effect of treatment, age, or genotype on the EDL elastic stiffness. * = genotype effect, # = age effects, @ = treatment effects, * = $p<0.05$ determined by two-way ANOVAs with post-hoc Sidak multiple comparisons tests.
(TIF)

S2 Fig. Sirius Red collagen architecture relates to muscle elasticity. (A-B) There were no significant main effects determined by three-way ANOVAs across treatment, genotype, and age for EDL and soleus muscle MicroECM alignment and MacroECM deviation. (C) MicroECM alignment of overall and *mdx* soleus muscles scaled negatively with elastic index. (D) MacroECM deviation demonstrated a weak positive correlation with elastic index across all muscles.
(TIF)

S3 Fig. Soleus collagen architecture and sarcomere length. *Mdx* soleus has greater collagen alignment and sarcomere length relates to elastic stiffness. (A) Second Harmonic Generation (SHG) representative images of soleus muscle sections from young, adult, wildtype, and *mdx* mice. Colormap represents angles of each pixel window in the images as analyzed by OrientationJ. Scale bar is 100μm. (B) Adult solei had higher collagen fiber area than young solei. (C) Adult and *mdx* solei had lower collagen deviation (higher alignment) than young and wildtype solei. (D) Adult diaphragm muscles had longer sarcomere lengths than young diaphragms, and wildtype solei had longer sarcomere lengths than *mdx*. (E) Adult soleus muscles had larger mean collagen fiber diameters than young soleus muscles. (F) Collagen deviation had a positive correlation with sarcomere length across all muscles and in the diaphragm. (G) There was a significant positive correlation between sarcomere length and elastic stiffness across all groups. (H) There was no significant correlation between collagen fiber diameter and elastic stiffness. Significance bars represent significant main effects determined by three-way ANOVAs for treatment, genotype, and age. Significance symbol above groups indicates significance from corresponding genotype or age according to post-hoc Sidak multiple comparisons tests. Significance by genotype: *$p<0.05$ and age: #$p<0.05$.
(TIF)

S4 Fig. Correlation matrices demonstrated significant linear relationships between endpoint parameters across and within muscles. (A) Correlation matrix showing significant relationships between parameters across all muscles. (B-D) Correlation matrices of individual muscles showing significant relationships between parameters in diaphragm, EDL, and soleus muscles. *$p<0.05$, determined by Pearson correlation analysis.
(TIF)

S5 Fig. Multiple Linear Regressions show significant relationships between collagen architecture and specific tension/passive stiffness. (A) The combined model produced insoluble collagen as a negative predictor of specific tension. (B) The model gave collagen deviation as a positive predictor for specific tension in EDL and insoluble collagen as a negative predictor. (C) The model gave sarcomere length as the only positive predictor for specific tension in soleus. (D-I) Multiple linear regressions of young and adult groups of muscles demonstrated significant predictors of elastic stiffness. (J-M) Multiple linear regressions of combined and individual muscles showed collagen architecture relates to dynamic stiffness.
(TIF)

Acknowledgments

The UC Davis Health Sciences District Advanced Imaging Facility and Dr. Ingrid Brust-Mascher supported the SHG Imaging. The work was supported by the lab Dr. Keith Baar including access to equipment and attentive comments on the study. We would like to thank Xinyue Li for support in preparation of the manuscript and thoughtful discussions. We would also like to thank additional members of the MyoMatrix Lab at UC Davis including CJ Mileti, Taryn Loomis, Daryl Dinh, and Matthew Nakaki for insightful conversations and review of the data.

Author Contributions

Conceptualization: Sarah E. Brashear, Lucas R. Smith.

Data curation: Sarah E. Brashear, Ross P. Wohlgemuth, Lin-Ya Hu.

Formal analysis: Sarah E. Brashear, Ross P. Wohlgemuth, Elias H. Jbeily, Lucas R. Smith.

Funding acquisition: Lucas R. Smith.

Investigation: Sarah E. Brashear, Ross P. Wohlgemuth, Lin-Ya Hu, Elias H. Jbeily.

Methodology: Sarah E. Brashear, Ross P. Wohlgemuth, Lin-Ya Hu, Elias H. Jbeily, Blaine A. Christiansen, Lucas R. Smith.

Project administration: Lucas R. Smith.

Resources: Lucas R. Smith.

Software: Ross P. Wohlgemuth.

Supervision: Lin-Ya Hu, Blaine A. Christiansen, Lucas R. Smith.

Validation: Ross P. Wohlgemuth.

Visualization: Sarah E. Brashear, Ross P. Wohlgemuth, Elias H. Jbeily, Blaine A. Christiansen.

Writing – original draft: Sarah E. Brashear, Ross P. Wohlgemuth.

Writing – review & editing: Sarah E. Brashear, Ross P. Wohlgemuth, Lin-Ya Hu, Elias H. Jbeily, Blaine A. Christiansen, Lucas R. Smith.

References

1. HERBERT R. The Passive Mechanical Properties of Muscle and Their Adaptations to Altered Patterns of Use. Australian Journal of Physiotherapy 1988; 34:141–9. https://doi.org/10.1016/S0004-9514(14)60606-1 PMID: 25026068
2. Meyer G, Lieber RL. Muscle fibers bear a larger fraction of passive muscle tension in frogs compared with mice. Journal of Experimental Biology 2018; 221. https://doi.org/10.1242/jeb.182089.

3. Ward SR, Winters TM, O'Connor SM, Lieber RL. Non-linear Scaling of Passive Mechanical Properties in Fibers, Bundles, Fascicles and Whole Rabbit Muscles. Front Physiol 2020; 11. https://doi.org/10.3389/FPHYS.2020.00211. PMID: 32265730
4. Gillies AR, Lieber RL. Structure and function of the skeletal muscle extracellular matrix. Muscle Nerve 2011; 44:318–31. https://doi.org/10.1002/mus.22094 PMID: 21949456
5. Wang H, Abhilash AS, Chen CS, Wells RG, Shenoy VB. Long-range force transmission in fibrous matrices enabled by tension-driven alignment of fibers. Biophys J 2015; 107:2592–603. https://doi.org/10.1016/j.bpj.2014.09.044.
6. Granzier HL, Irving TC. Passive tension in cardiac muscle: contribution of collagen, titin, microtubules, and intermediate filaments. Biophys J 1995; 68:1027. https://doi.org/10.1016/S0006-3495(95)80278-X PMID: 7756523
7. Bonnans C, Chou J, Werb Z. Remodelling the extracellular matrix in development and disease. Nat Rev Mol Cell Biol 2014; 15:786–801. https://doi.org/10.1038/nrm3904 PMID: 25415508
8. Smith LR, Lee KS, Ward SR, Chambers HG, Lieber RL. Hamstring contractures in children with spastic cerebral palsy result from a stiffer extracellular matrix and increased in vivo sarcomere length. Journal of Physiology 2011; 589:2625–39. https://doi.org/10.1113/jphysiol.2010.203364 PMID: 21486759
9. Elder GCB, Stewart G, Cook K, Weir D, Marshall A, Leahey L. Contributing factors to muscle weakness in children with cerebral palsy. Dev Med Child Neurol 2003; 45:542–50. https://doi.org/10.1017/s0012162203000999 PMID: 12882533
10. Skalsky AJ, McDonald CM. Prevention and management of limb contractures in neuromuscular diseases. Phys Med Rehabil Clin N Am 2012; 23:675–87. https://doi.org/10.1016/j.pmr.2012.06.009 PMID: 22938881
11. Cheeran D, Khan S, Khera R, Bhatt A, Garg S, Grodin JL, et al. Predictors of Death in Adults With Duchenne Muscular Dystrophy-Associated Cardiomyopathy. J Am Heart Assoc 2017; 6. https://doi.org/10.1161/JAHA.117.006340 PMID: 29042427
12. Wynn TA. Cellular and molecular mechanisms of fibrosis. J Pathol 2008; 214:199–210. https://doi.org/10.1002/path.2277 PMID: 18161745
13. Huebner KD, Jassal DS, Halevy O, Pines M, Anderson JE. Functional resolution of fibrosis in mdx mouse dystrophic heart and skeletal muscle by halofuginone. Am J Physiol Heart Circ Physiol 2008; 294. https://doi.org/10.1152/ajpheart.01253.2007 PMID: 18263710
14. Brashear SE, Wohlgemuth RP, Gonzalez G, Smith LR. Passive stiffness of fibrotic skeletal muscle in mdx mice relates to collagen architecture. J Physiol 2021; 599:943–62. https://doi.org/10.1113/JP280656 PMID: 33247944
15. Smith LR, Barton ER. Collagen content does not alter the passive mechanical properties of fibrotic skeletal muscle in mdx mice. Am J Physiol Cell Physiol 2014; 306:C889–98. https://doi.org/10.1152/ajpcell.00383.2013 PMID: 24598364
16. Smith LR, Hammers DW, Sweeney HL, Barton ER. Increased collagen cross-linking is a signature of dystrophin-deficient muscle. Muscle Nerve 2016; 54:71–8. https://doi.org/10.1002/mus.24998 PMID: 26616495
17. Baker AM, Bird D, Lang G, Cox TR, Erler JT. Lysyl oxidase enzymatic function increases stiffness to drive colorectal cancer progression through FAK. Oncogene 2013; 32:1863–8. https://doi.org/10.1038/onc.2012.202 PMID: 22641216
18. Garnero P. The contribution of collagen crosslinks to bone strength. Bonekey Rep 2012; 1:182. https://doi.org/10.1038/bonekey.2012.182 PMID: 24363926
19. Ikenaga N, Peng ZW, Vaid KA, Liu SB, Yoshida S, Sverdlov DY, et al. Selective targeting of lysyl oxidase-like 2 (LOXL2) suppresses hepatic fibrosis progression and accelerates its reversal. Gut 2017; 66:1697–708. https://doi.org/10.1136/gutjnl-2016-312473 PMID: 28073888
20. Liu SB, Ikenaga N, Peng ZW, Sverdlov DY, Greenstein A, Smith V, et al. Lysyl oxidase activity contributes to collagen stabilization during liver fibrosis progression and limits spontaneous fibrosis reversal in mice. FASEB Journal 2016; 30:1599–609. https://doi.org/10.1096/fj.14-268425 PMID: 26700732
21. Eyre DR, Weis MA, Rai J. Analyses of lysine aldehyde cross-linking in collagen reveal that the mature cross-link histidinohydroxylysinonorleucine is an artifact. J Biol Chem 2019; 294:6578. https://doi.org/10.1074/jbc.RA118.007202 PMID: 30733334
22. Paul RG, Bailey AJ. Glycation of collagen: the basis of its central role in the late complications of ageing and diabetes. Int J Biochem Cell Biol 1996; 28:1297–310. https://doi.org/10.1016/s1357-2725(96)00079-9 PMID: 9022289
23. Tang SS, Trackman PC, Kagan HM. Reaction of aortic lysyl oxidase with beta-aminopropionitrile. Journal of Biological Chemistry 1983; 258:4331–8. https://doi.org/10.1016/S0021-9258(18)32627-9. PMID: 6131892

24. Mcnerny EM, Gong B, Morris MD, Kohn DH. Bone Fracture Toughness and Strength Correlate With Collagen Cross-Link Maturity in a Dose-Controlled Lathyrism Mouse Model 2014. https://doi.org/10.1002/jbmr.2356.

25. Novotny SA, Warren GL, Lin AS, Guldberg RE, Baltgalvis KA, Lowe DA. Bone is functionally impaired in dystrophic mice but less so than skeletal muscle. Neuromuscular Disorders 2011; 21:183–93. https://doi.org/10.1016/j.nmd.2010.12.002 PMID: 21256750

26. van Putten M, Putker K, Overzier M, Adamzek WA, Pasteuning-Vuhman S, Plomp JJ, et al. Natural disease history of the D2-mdx mouse model for Duchenne muscular dystrophy. FASEB Journal 2019; 33:8110–24. https://doi.org/10.1096/fj.201802488R PMID: 30933664

27. Hammers DW, Hart CC, Matheny MK, Wright LA, Armellini M, Barton ER, et al. The D2.mdx mouse as a preclinical model of the skeletal muscle pathology associated with Duchenne muscular dystrophy. Sci Rep 2020; 10:1–12. https://doi.org/10.1038/s41598-020-70987-y.

28. El Hajj EC, El Hajj MC, Ninh VK, Gardner JD. Cardioprotective effects of lysyl oxidase inhibition against volume overload-induced extracellular matrix remodeling. Exp Biol Med (Maywood) 2016; 241:539–49. https://doi.org/10.1177/1535370215616511 PMID: 26582054

29. Barton ER, Morris L, Kawana M, Bish LT, Toursel T. Systemic administration of L-arginine benefits mdx skeletal muscle function. Muscle Nerve 2005; 32:751–60. https://doi.org/10.1002/mus.20425 PMID: 16116642

30. Petrof BJ, Stedman HH, Shrager JB, Eby J, Sweeney HL, Kelly AM. Adaptations in myosin heavy chain expression and contractile function in dystrophic mouse diaphragm. Am J Physiol 1993; 265. https://doi.org/10.1152/ajpcell.1993.265.3.C834 PMID: 8214039

31. Moorwood C, Liu M, Tian Z, Barton ER. Isometric and eccentric force generation assessment of skeletal muscles isolated from murine models of muscular dystrophies. Journal of Visualized Experiments 2013: 50036. https://doi.org/10.3791/50036 PMID: 23407283

32. Mendez J, Keys A. Density and composition of mammalian muscle. Metabolism 1960; 9:184–8.

33. Burkholder TJ, Lieber RL. REVIEW SARCOMERE LENGTH OPERATING RANGE OF VERTEBRATE MUSCLES DURING MOVEMENT. vol. 204. 2001.

34. Hakim CH, Grange RW, Duan D. The passive mechanical properties of the extensor digitorum longus muscle are compromised in 2- to 20-mo-old mdx mice. J Appl Physiol 2011; 110:1656–63. https://doi.org/10.1152/japplphysiol.01425.2010 PMID: 21415170

35. Ward SR, Tomiya A, Regev GJ, Thacker BE, Benzl RC, Kim CW, et al. Passive mechanical properties of the lumbar multifidus muscle support its role as a stabilizer. J Biomech 2009; 42:1384–9. https://doi.org/10.1016/j.jbiomech.2008.09.042 PMID: 19457491

36. Flesch M, Schiffer F, Zolk O, Pinto Y, Rosenkranz S, Hirth-Dietrich C, et al. Contractile Systolic and Diastolic Dysfunction in Renin-Induced Hypertensive Cardiomyopathy. Hypertension 1997; 30:383–91. https://doi.org/10.1161/01.hyp.30.3.383 PMID: 9314421

37. Heydemann A, Huber JM, Demonbreun A, Hadhazy M, McNally EM. Genetic background influences muscular dystrophy. Neuromuscular Disorders 2005; 15:601–9. https://doi.org/10.1016/j.nmd.2005.05.004 PMID: 16084087

38. Acuña M, Pessina P, . . . HO-H molecular, 2014 undefined. Restoration of muscle strength in dystrophic muscle by angiotensin-1-7 through inhibition of TGF-β signalling. AcademicOupCom n.d.

39. Trensz F, Haroun S, Cloutier A, Richter M V., Grenier G. A muscle resident cell population promotes fibrosis in hindlimb skeletal muscles of mdx mice through the Wnt canonical pathway. American Journal of Physiology-Cell Physiology 2010; 299:C939–47. https://doi.org/10.1152/ajpcell.00253.2010.

40. Hu LY, Mileti CJ, Loomis T, Brashear SE, Ahmad S, Chellakudam RR, et al. Skeletal muscle progenitors are sensitive to collagen architectural features of fibril size and cross linking. Am J Physiol Cell Physiol 2021; 321:C330–42. https://doi.org/10.1152/ajpcell.00065.2021 PMID: 34191625

41. Bouxsein ML, Boyd SK, Christiansen BA, Guldberg RE, Jepsen KJ, Mü Ller R. Guidelines for Assessment of Bone Microstructure in Rodents Using Micro-Computed Tomography n.d. https://doi.org/10.1002/jbmr.141.

42. Jepsen KJ, Silva MJ, Vashishth D, Guo XE, Ch Van Der Meulen M. Establishing Biomechanical Mechanisms in Mouse Models: Practical Guidelines for Systematically Evaluating Phenotypic Changes in the Diaphyses of Long Bones 2015. https://doi.org/10.1002/jbmr.2539 PMID: 25917136

43. Stedman HH, Sweeney HL, Shrager JB, Maguire HC, Panettieri RA, Petrof B, et al. The mdx mouse diaphragm reproduces the degenerative changes of Duchenne muscular dystrophy. Nature 1991 352:6335 1991; 352:536–9. https://doi.org/10.1038/352536a0 PMID: 1865908

44. Pennati F, Arrigoni F, LoMauro A, Gandossini S, Russo A, D'Angelo MG, et al. Diaphragm Involvement in Duchenne Muscular Dystrophy (DMD): An MRI Study. J Magn Reson Imaging 2020; 51:461–71. https://doi.org/10.1002/jmri.26864 PMID: 31301202

45. LoMauro A, Romei M, Gandossini S, Pascuzzo R, Vantini S, D'Angelo MG, et al. Evolution of respiratory function in Duchenne muscular dystrophy from childhood to adulthood. Eur Respir J 2018; 51. https://doi.org/10.1183/13993003.01418-2017.

46. Spaulding HR, Quindry T, Quindry JC, Selsby JT. Nutraceutical and pharmaceutical cocktails did not preserve diaphragm muscle function or reduce muscle damage in D2-mdx mice. Exp Physiol 2020; 105:989–99. https://doi.org/10.1113/EP087887 PMID: 32267561

47. Meyer GA, Lieber RL. Elucidation of extracellular matrix mechanics from muscle fibers and fiber bundles. J Biomech 2011; 44:771–3. https://doi.org/10.1016/j.jbiomech.2010.10.044 PMID: 21092966

48. Gillies AR, Chapman MA, Bushong EA, Deerinck TJ, Ellisman MH, Lieber RL. High resolution three-dimensional reconstruction of fibrotic skeletal muscle extracellular matrix. Journal of Physiology 2017; 595:1159–71. https://doi.org/10.1113/JP273376 PMID: 27859324

49. Chapman MA, Pichika R, Lieber RL. Collagen crosslinking does not dictate stiffness in a transgenic mouse model of skeletal muscle fibrosis. J Biomech 2015; 48:375–8. https://doi.org/10.1016/j.jbiomech.2014.12.005 PMID: 25529136

50. Sahani R, Wallace CH, Jones BK, Blemker SS. Diaphragm muscle fibrosis involves changes in collagen organization with mechanical implications in Duchenne Muscular Dystrophy. Https://DoiOrg/101152/Japplphysiol002482021 2022. https://doi.org/10.1152/JAPPLPHYSIOL.00248.2021.

51. Lopez MA, Bontiff S, Adeyeye M, Shaibani AI, Alexander MS, Wynd S, et al. Mechanics of dystrophin deficient skeletal muscles in very young mice and effects of age. Am J Physiol Cell Physiol 2021; 321: C230–46. https://doi.org/10.1152/ajpcell.00155.2019 PMID: 33979214

52. Canelón SP, Wallace JM. Substrate Strain Mitigates Effects of β-Aminopropionitrile-Induced Reduction in Enzymatic Crosslinking. Calcif Tissue Int 2019; 105:660–9. https://doi.org/10.1007/s00223-019-00603-3 PMID: 31482192

53. Izawa-Ishizawa Y, Imanishi M, Zamami Y, Toya H, Nagao T, Morishita M, et al. Development of a novel aortic dissection mouse model and evaluation of drug efficacy using in-vivo assays and database analyses. J Hypertens 2019; 37:73–83. https://doi.org/10.1097/HJH.0000000000001898 PMID: 30303488

54. Shen Y, Jing D, Hao J, Tang G, Yang P, Zhao Z. The Effect of β-Aminopropionitrile on Skeletal Micromorphology and Osteogenesis. Calcif Tissue Int 2018; 103:411–21. https://doi.org/10.1007/s00223-018-0430-4 PMID: 29916126

55. McNerny EMB, Gong B, Morris MD, Kohn DH. Bone fracture toughness and strength correlate with collagen cross-link maturity in a dose-controlled lathyrism mouse model. J Bone Miner Res 2015; 30:446–55. https://doi.org/10.1002/JBMR.2356.

56. Chen W, Yang A, Jia J, Popov Y V., Schuppan D, You H. Lysyl Oxidase (LOX) Family Members: Rationale and Their Potential as Therapeutic Targets for Liver Fibrosis. Hepatology 2020; 72:729–41. https://doi.org/10.1002/hep.31236 PMID: 32176358

57. Zhao W, Yang A, Chen W, Wang P, Liu T, Cong M, et al. Inhibition of lysyl oxidase-like 1 (LOXL1) expression arrests liver fibrosis progression in cirrhosis by reducing elastin crosslinking. Biochim Biophys Acta Mol Basis Dis 2018; 1864:1129–37. https://doi.org/10.1016/j.bbadis.2018.01.019 PMID: 29366776

58. Stangenberg S, Saad S, Schilter HC, Zaky A, Gill A, Pollock CA, et al. Lysyl oxidase-like 2 inhibition ameliorates glomerulosclerosis and albuminuria in diabetic nephropathy. Sci Rep 2018; 8. https://doi.org/10.1038/s41598-018-27462-6 PMID: 29930330

59. Thompson NS, Baker RJ, Cosgrove AP, Corry IS, Graham HK. Musculoskeletal modelling in determining the effect of botulinum toxin on the hamstrings of patients with crouch gait. Dev Med Child Neurol 1998; 40:622–5. https://doi.org/10.1111/j.1469-8749.1998.tb15428.x PMID: 9766740

60. Cosgrove D, Dufek B, Meehan DT, Delimont D, Hartnett M, Samuelson G, et al. Lysyl oxidase like-2 contributes to renal fibrosis in Col4α3/Alport mice. Kidney Int 2018; 94:303–14. https://doi.org/10.1016/j.kint.2018.02.024 PMID: 29759420

61. Wang H, Poe A, Pak L, Nandakumar K, Jandu S, Steppan J, et al. An in situ activity assay for lysyl oxidases. Commun Biol 2021; 4. https://doi.org/10.1038/s42003-021-02354-0.